The importance of resolving nearshore currents in coastal dispersal models

Ward, Sophie; Robins, Peter; Owen, Aaron; Demmer, Jonathan; Jenkins, Stuart

Ocean Modelling

Published: 01/06/2023

Peer reviewed version

The importance of resolving nearshore currents in coastal dispersal models

Ward, S.L.[1], Robins, P.E.[1], Owen, A.[2], Demmer, J.[1], and Jenkins S.R.[1]

Affiliations:

[1]School of Ocean Sciences, Bangor University, Menai Bridge, Isle of Anglesey, LL59 5AB, UK

[2]Digital Services, Bangor University, Bangor, LL57 2DG, UK

Abstract

Biophysical models often require shelf-scale domains to map larval dispersal over several weeks, presenting a computational challenge. This can be overcome by decreasing model spatial resolution; however, nearshore processes, which potentially play a significant role in larval dispersal, will inevitably be unresolved. Here, we evaluate how simulated larval dispersal in the nearshore is sensitive to model spatial resolution. We use an unstructured, finite element, hydrodynamic model of a topographically-complex coastline in North Wales, UK (which includes headlands, bays and channels) at four different spatial scales (50, 100, 250, 500 m) to compare the influence of spatial resolution on transport and dispersal patterns of particles released within the nearshore region (within 1 km of the shore). In the higher resolution (50 and 100 m) simulations, particles generally travelled offshore more quickly and further (~18%) than in the coarser (250 and 500 m) simulations. This had important implications for potential connectivity along the coast: for the lower resolution simulations, retention of particles near source sites was increased by ~50% and, whilst the magnitude of connectivity among discrete regions along the coast was also increased (by ~27%), the number of connected regions was reduced (by ~9%), compared with the higher resolution simulations. Our results, based on a case study in a highly energetic and topographically complex region, suggest that model spatial resolution of ≤100 m should be used for dispersal studies in the nearshore zone. These findings add to growing evidence of the importance of using appropriately scaled models when simulating the transport of material within- and out of- the coastal zone, with many applications, such as marine ecology, marine biosecurity, marine spatial planning and marine pollution.

Keywords: *Coastal currents; dispersion; Lagrangian analysis; ocean model; connectivity; North Wales*

1 Introduction

The life cycle of the majority of marine organisms begins with pelagic stages (e.g., larvae, eggs, spores), which are non- or weak-swimming and hence whose fate is determined by physical transport processes (Lester and Ruttenberg, 2005; Shanks, 2009; Simons et al., 2013). For many benthic organisms, these early-life stages are their only chance for population and genetic connectivity. Understanding dispersal within the marine environment is an inherently difficult problem, as both intrinsic (e.g., swimming behaviour, pelagic larval duration, mortality) and extrinsic (e.g., ocean currents) factors influence dispersal trajectories (Pineda et al., 2007). Because larvae are small, obtaining *in-situ* observations of their dispersal patterns is challenging and generally impractical (but see Davis and Butler, 1989). In lieu of observational data, biophysical models (also referred to as particle tracking models) use simulations from hydrodynamic models of the evolution of ocean currents and mixing rates to estimate the potential Lagrangian transport of particles (in this case larvae). These models can predict the potential dispersal of millions of 'virtual larvae' under a range of environmental conditions and biological traits. A valuable application of particle tracking models is to simulate larval transport from source to sink, i.e., from the natal population to a suitable settlement location, hence predicting the pattern and magnitude of population connectivity.

There are a number of uncertainties associated with larval dispersal modelling. Some of these uncertainties are biological in nature (e.g., unknowns and variabilities in their pelagic larval duration and behaviour within the water column or during settlement), while others are related to the uncertainties in the representation of the physical environment (e.g., model resolution and model parameterisation). Although several studies have considered the sensitivity of propagule dispersal to a range of physical/biological processes and model parameterisations (Hufnagl et al., 2017; Robins et al., 2013; Simons et al., 2013; Treml et al., 2015), there remains no 'one size fits all' approach to estimating larval transport and dispersal. As a baseline (regardless of the complexity of either known- or estimated larval life history traits), biophysical models should be driven by physical parameters that have been simulated at appropriate spatio-temporal resolutions for the question in-hand.

Many benthic invertebrate taxa, as well as both pelagic and demersal fish, spawn in coastal regions which exhibit a complex flow regime, influenced by tides, rivers, wind and waves. These energetic and dynamic physical coastal processes have implications for the transport and dispersal of larvae, as currents interact with undulating topographic features and channels (Vasile et al., 2018) to produce local residual flows such as tidally-asymmetric currents; longshore currents (Nickols et al., 2012); rip currents (Fujimura et al., 2014; Largier, 2003;

Morgan et al., 2018; Talbot and Bate, 1987); upwelling (Dauhajre et al., 2019; Suanda et al., 2018); recirculating eddies estuarine circulation (Kim et al., 2010; Pastor et al., 2018); and axial convergent fronts (Robins et al., 2012). The role of active swimming in determining patterns of dispersal is variable, but generally low, and certainly for the period directly after spawning, larvae tend to behave passively (Drake et al., 2018). Hence for nearshore taxa, coastal currents are critical in determining transport, and the likelihood of dispersal offshore. However, coastal currents and turbulent mixing can vary greatly over small spatial and temporal scales, especially near undulating coastlines and islands, and consequently their role in dispersing larvae is poorly understood at present (Dauhajre et al., 2019; Drake et al., 2018; Morgan et al., 2018; Nickols et al., 2012).

Particle tracking models have been developed over a variety of spatio-temporal scales (e.g., Dauhajre et al., 2019; Demmer et al., 2022; Lynge et al. 2010; Ricker and Stanev, 2020; Vasile et al., 2018). Whilst model spatial resolution has generally increased over the past few decades there has been a lack of consistency in approach (Swearer et al., 2019) with a trade-off between increasing resolution and model extent owing to computational limitations. Larval dispersal over several weeks has the potential to connect distant populations, hundreds of kilometres apart. Hence modelling approaches have typically adopted coarse resolution (1-5 km) 3D models to cover these large distances within computational constraints (e.g., Bode et al., 2019; Drake et al., 2018; King et al., 2020; Torrado et al., 2021). Being focussed on offshore circulation, these coarse models often do not resolve coastal dynamics. However, computational capacity is now at the stage where mesoscale (of the order 100 km) models can resolve coastal currents at appropriate resolution (e.g., <50 m). This capacity is necessary for dispersal studies of coastal species that need to simulate larval transport in coastal environments as well as long-distance offshore dispersal pathways. Therefore, there is a need to better-understand the influence on model spatial resolution on simulated larval dispersal patterns, so that a standardised approach can be designed for future studies.

We hypothesise that nearshore residual currents tend to restrict the offshore dispersal of larvae spawned within the coastal zone. Therefore, biophysical models that do not accurately resolve nearshore residual currents may over-estimate offshore dispersal and population connectivity. We compare the relative transport and dispersal of particles released from a topographically-complex and tidally-energetic coastline, using five hydrodynamic models of different spatial resolutions. We aim to explore this uncertainty within the context of other uncertainties in dispersal due to oceanographic conditions and pelagic larval duration.

2 Methods

We applied a hydrodynamic model to five different mesh configurations to investigate how spatial resolution influenced our estimations of particle dispersal within the coastal zone (see Section 2.1). These model domains covered a section of topographically complex coastline of North Wales, UK, located within the Irish Sea. The model domain was selected as it encompasses a variety of hydrodynamic conditions over a short domain (e.g., energetic flows around headlands, quiescent water within bays, tidally asymmetric flow through channels and recirculating flows around islands). The stretch of coast also varies in aspect relative to the predominant tidal flow. Further, the North Wales coastline is well-developed, with numerous anthropogenic activities within the coastal region, e.g., harbours, marinas, a major seaport (Holyhead), fishing activities, tourism, sea defences, as well as offshore renewable energy infrastructure. The hydrodynamics of the Irish Sea are driven mainly by tidal currents (Robinson, 1979) and the coastal waters remain well-mixed throughout the year. The tidal range reaches 8.6 m at Llandudno (tide gauge B, Figure 1a), and tidal currents can exceed 3 m s^{-1} off headlands of northwest Anglesey, where mean water depth is up to 40 m within 1 km of the shore. Along much of the coastline in the region, the mean water depth remains <10 m (up to 1 km offshore), with large intertidal zones in many of the bays.

We developed a particle tracking model, coded in MATLAB (version R2020a), and run on a supercomputer (Supercomputing Wales), that used the simulated coastal currents to advect particles within the coastal region (see Section 2.2). We considered the implications of using relatively low- (hundreds of metres) and high- (tens of metres) resolution hydrodynamic models of coastal regions on the transport and resulting dispersal patterns of particles. These particles were representative of passive larvae, and here we consider their dispersal from nearshore release locations, for up to two weeks from spawning. This period is relevant to a huge range of coastal benthic invertebrate species living in shallow coastal regions with a pelagic duration of two weeks or more (see O'Connor et al., 2007 for a review). For those taxa with long pelagic larval duration, such as many crustaceans and molluscs, this period represents the early-stage larvae/eggs when active swimming (or other behaviours) tends to be extremely limited.

2.1 Hydrodynamic model

We applied TELEMAC to our different grid configurations, which is an open-source hydrodynamic modelling system (www.opentelemac.org) – specifically TELEMAC-2D (version 8p2r0). This model solves the Shallow Water Equations (Saint-Venant equations) in two-dimensions (depth-averaged), using finite element or finite volume methods (Hervouet, 2000),

which is a good approximation for the dominant barotropic flows of the region, where mean spring tidal ranges are >6 m (Robinson, 1979; Horrillo-Caraballo et al., 2021), see Section 2.2, model validation. The hydrodynamic model was run in finite element mode, based on unstructured triangular computational mesh grids, facilitating increased model resolution in nearshore regions, with coarser resolution offshore. This unstructured grid capability maximises the resolution of coastal processes while optimising computational efficiency. The model included alternate wetting and drying of model nodes in the inter-tidal regions and is therefore a sound choice for shallow coastal domains (e.g., Robins et al., 2014; Davies and Robins, 2017).

We developed five model configurations of the North Wales coastal region, with different horizontal spatial resolutions in the nearshore zone (Figure 2) 50 m (R50), 100 m (R100), 250 m (R250), and 500 m (R500). In each model configuration, all triangular elements between the shoreline and 1 km were constrained to not exceed one of 50/100/250/500 m in edge length, as focus was on the difference in model resolution in the coastal region. The mesh edge lengths were each set to increase to 750 m by 20 km offshore (the rate of edge length growth depending on the nearshore resolution), after which mesh edge lengths extended to ~3 km at the model boundary. A fifth grid was generated, of the same spatial resolution as the highest resolution grid (R50), the purpose being to confirm that any differences in particle transport simulation was a consequence of hydrodynamic mesh resolution rather than configuration (see Results section). This fifth grid was constrained in the same way as described above (50 m resolution within 1 km from shore increasing to 750 m within 20 km from shore), but the mesh-generator was re-run so that individual triangular elements were configured differently to R50. Bathymetric data comprised data from EMODnet (www.emodnet-bathymetry.eu) and the UK Hydrographic Office ADMIRALTY Marine Data Portal. First, the lower resolution 2018 EMODnet Digital Terrain Model (grid resolution of 1/16 × 1/16 arc minutes, ~115 m) were interpolated onto each grid, over which the high resolution (2 – 4 m) UK Hydrographic Office multibeam data (www.admiralty.co.uk) were mapped, where available. These datasets were used as they were the highest resolution bathymetric datasets which covered the entire model domain.

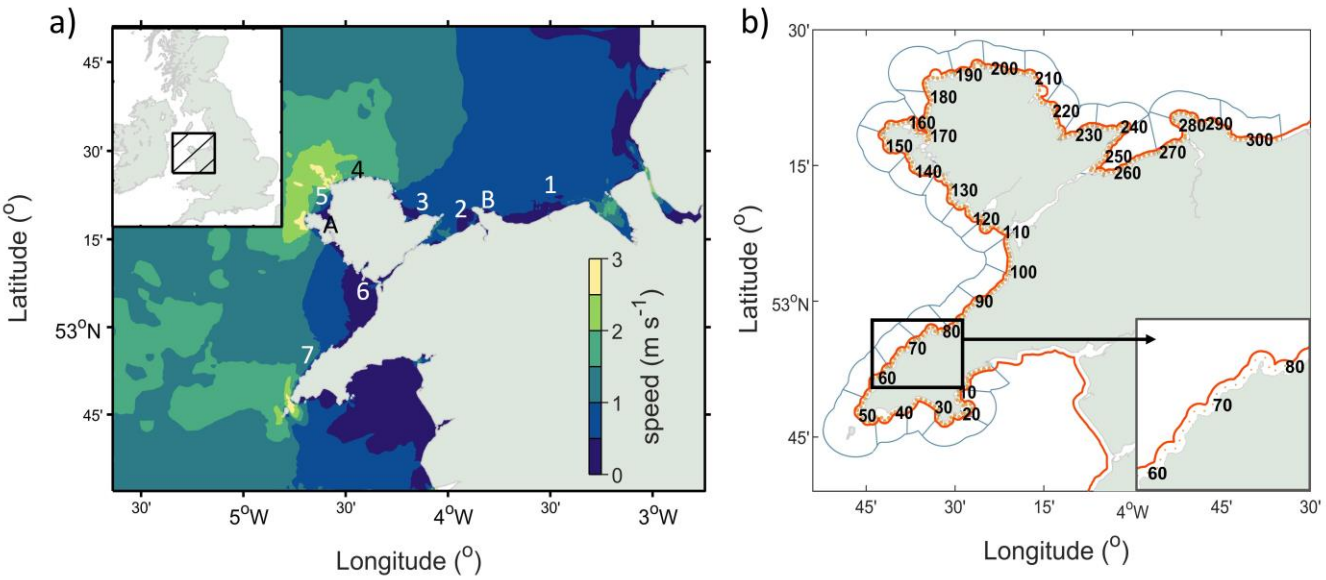

177 ***Figure 1. a) Model domain (wider context given in inset map) showing simulated peak***
178 ***tidal current speeds, and locations of ADCPs (numbers) and coastal tide gauges***
179 ***(letters) used in the model validation. The model domain is ~200 km east-west and***
180 ***~150 km north-south. b) Release points (orange dots and numbers) and 1 km offshore***
181 ***boundary (red line), blue lines outline the 30 zones used in the estimation of alongshore***
182 ***connectivity.***

183

184 The model was forced by tidal boundary conditions, with no other forcing, i.e., neglecting wind-
185 and wave-driven currents, river plumes, density fields, etc. The potential implications of this
186 approach are discussed in Section 4.2. The tides in the Irish Sea are dominated by M_2 and S_2
187 (principle semi-diurnal lunar and solar, respectively) constituents, with K_1 (diurnal luni-solar),
188 O_1 (diurnal lunar) and N_2 (lunar ecliptic semi-diurnal) being relatively important in some
189 regions. The models described here were forced at the open boundaries using tidal elevation
190 amplitudes and velocities of 15 harmonic constituents (M_2, S_2, N_2, K_2, K_1, O_1, P_1, Q_1, M_4, MS_4,
191 MN_4, Mf, Mm $2N_2$ and S_1) derived from TPXO9 (TOPEX/Poseidon) global tide data which was
192 1/30 x 1/30 degree resolution ([www.tpxo.net/global/tpxo9-atlas]). For parameterisation of
193 friction, a constant friction coefficient of 0.025 was used in Nikuradse's law of bottom friction
194 (Hervouet, 2000). The model was parameterised to have a constant viscosity, both across the
195 domain and between model configurations. The model's velocity diffusivity coefficient was set
196 to 0.2, and this sets the value of the coefficient of viscosity (dynamic+turbulent) across the
197 domain. For both model stability as well as (to the greatest degree possible) maintaining a
198 consistent Courant-Friedrichs-Lewy (CFL) condition, the internal model timestep varied
199 between the simulations (1, 2, 5 and 10 s for R50, R100, R250 and R500, respectively). Each
200 model was run for a 42-day period, 40 days of which were output for analysis (including

harmonic analysis used in the model validation), which excluded two days of model spin-up, sufficient for tides-only simulations of this domain. Simulated water depth and u- and v-components of current velocity were output at TELEMAC-2D grid nodes at 15-minute (instantaneous) intervals.

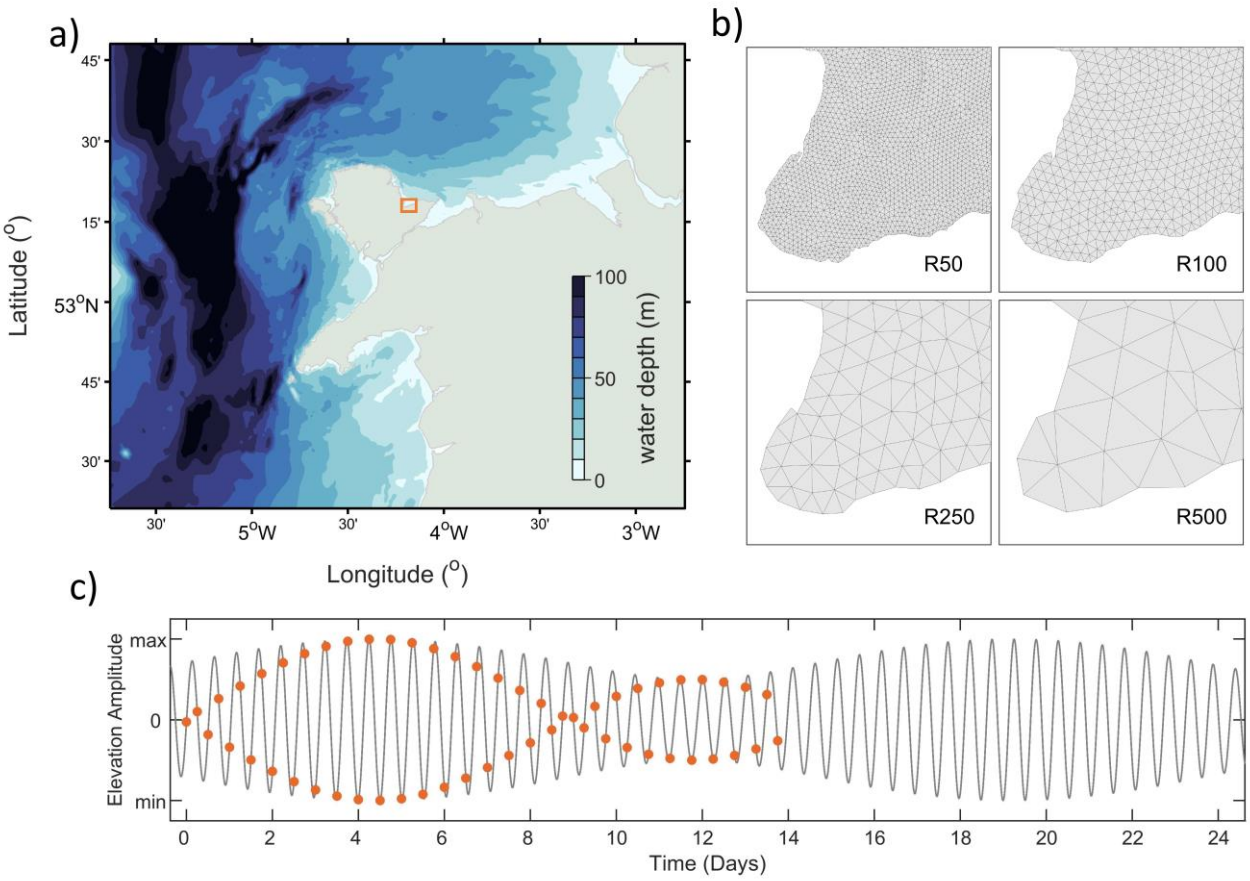

Figure 2. a) High resolution hydrodynamic model bathymetry (R50), orange square shows subsection in (b). b) Subsection of the model grids for R50, R100, R250 and R500 grids (grey lines). c) illustrating 56 x 6-hourly particle release times over a spring-neap cycle.

2.2 Hydrodynamic model validation

Simulated barotropic circulation was validated by comparing the two dominant constituents of the region (M_2 and S_2) with observational data (Table 1). Simulated tidal elevation amplitudes were compared with observed tidal elevation amplitudes at two coastal tide gauges within the region (Holyhead and Llandudno), and simulated tidal currents (Figure 3) were compared with observed tidal currents from (depth-averaged) current data collected by moored ADCPs (30-days of data were available) at seven points within the domain (Figure 1a). The bottom-mounted ADCPs were deployed in the nearshore zone, in both slow- and fast current

environments. Compared here are the decomposed (T_TIDE, Pawlowicz et al., 2002) amplitude and phase of the combined *uv* components of the M_2 and S_2 current speeds, calculated from the timeseries of both simulated- and observed depth-averaged currents. The comparison improved with finer model spatial resolution. Each grid configuration also validated well with regards elevation amplitude and phase; e.g., for R50, the root mean square error (RMSE) for two coastal tide gauges (Holyhead and Llandudno) was <1 cm (Scatter Index, SI=0.5%) in amplitude and 10° (SI=3%) in phase for M_2, and 5 cm (SI=2%) in amplitude and 14° (SI=4%) in phase for S_2, where the Scatter Index is the RMSE normalised by the mean of the data.

Table 1. Validation of simulated depth-averaged tidal currents (speeds and phases) for the dominant M_2 and S_2 tidal constituents, for models of different grid resolution

Validation of tidal currents		R50		R100		R250		R500	
		M_2	S_2	M_2	S_2	M_2	S_2	M_2	S_2
Speed	RMSE (cm/s)	6	2	7	2	8	3	9	3
	SI (%)	14	15	17	17	20	23	21	24
Phase	RMSE (◦)	12	15	12	16	12	17	12	17
	SI (%)	17	13	16	14	16	15	16	15

2.3 Lagrangian particle tracking model

An offline Lagrangian particle tracking model was developed in MATLAB (version 2020a) using the model outputs from the TELEMAC-2D simulations (available from: https://doi.org/10.5281/zenodo.7371420). Hypothetical particles were used to represent planktonic larvae and were advected (at 15-minute intervals) by the simulated tidal currents (magnitude and direction) from TELEMAC-2D. For consistency, this 15-minute hydrodynamic model output interval – and particle tracking model timestep - were the same between models of different resolutions. To ensure the runs were purely deterministic, thus enabling direct quantitative comparison, no additional sub-grid-scale diffusion (or 'random walk' term) was included in the particle tracking model. Generally speaking, for the relatively high resolution computational grids used here, additional stochastic models used to represent sub-grid scale diffusion processes are much less important than for coarser (e.g., kilometre-scale) models which do not resolve small-scale mixing processes (Marinone et al., 2007; Robins et al., 2013; Visser, 1997).

In TELEMAC-2D, which is based on vertex centred finite-element formulation, variables are defined at mesh nodes. At each time step, the velocities from the three nodes nearest to the particle location were barycentrically interpolated to the particle position (Equation 1). It is possible to calculate the barycentric coordinates of point P_1 inside a triangular element with three nodes N_1, N_2 and N_3, using:

$$\alpha_1 = \frac{Area\ of\ triangle\ \widehat{N_2PN_3}}{Area\ of\ triangle\ \widehat{N_1N_2N_3}}$$

$$\alpha_2 = \frac{Area\ of\ triangle\ \widehat{N_1PN_3}}{Area\ of\ triangle\ \widehat{N_1N_2N_3}}$$

$$\alpha_3 = \frac{Area\ of\ triangle\ \widehat{N_1PN_2}}{Area\ of\ triangle\ \widehat{N_1N_2N_3}}$$

Equation 1. Calculating barycentric coordinates (α_1 α_2 α_3) for point P within grid element with mesh nodes (N_1, N_2, N_3).

Where $N_1+N_2+N_3=1$. Using these barycentric coordinates, it is possible to interpolate the instantaneous velocity at point P_1:

$$UV(P_1) = \alpha_1 UV(N_1) + \alpha_2 UV(N_2) + \alpha_3 UV(N_3)$$

Equation 2. Instantaneous velocity, UV, interpolated to point P using barycentric coordinates.

This interpolated velocity, UV, is used to advect the particle from point P1, to point P2 for the period equal to the calculating timestep:

$$P_2 = P_1 + \delta t UV(P_1)$$

Equation 3. Iterative advection of particle position in time and space.

Particles were released 500 m offshore, at a spacing of ~1 km between release points along the North Wales coast (Figure 1b). The mean water depth in the model bathymetries at these sites 500 m offshore varied between 3 m (e.g., south coast of the Llŷn Peninsula) and 47 m (e.g., north coast of Anglesey). One particle was released from each location every 6 hours over 14 days (56 particles per site in total), to encompass particle releases throughout the spring-neap tidal cycle (Figure 2c). Each particle was set to propagate for 14 days of pelagic transport. The particles simulated were entirely passive, i.e., density and behavioural complexity were omitted, as the focus here is on how physical hydrodynamic processes affect

dispersal. As such, these analyses did not include differential distribution in the water column through larval swimming or particles sinking/rising. Particles were sometimes advected onto 'land' (referred to later as "interactions" with the coastline), where land was defined as a minimum water depth of 0.1 m. When this occurred, particles were returned to their position during the previous timestep. This approach, similarly employed in previous studies (e.g., Coscia et al., 2020), was necessary to avoid particles getting stranded on 'land' (which also includes particles being beached due to model wetting and drying), in particular soon after release from the coastal release points. This method was a compromise between computational capacity and realistic simulation.

To quantify the difference in Lagrangian transport between individual particle trajectories on the different grid configurations, we calculated the root mean square error (RMSE) for each particle trajectory, from R100, R250 and R500, relative to the corresponding particle trajectory from the R50 simulations, using:

$$RMSE = \sqrt{\frac{\sum_{i=1}^{n}(R50_i - RX_i)^2}{n}}$$

Where RX is either R100, R250 or R500, $i = 1{:}n$ where n is the number of logged trajectory points (i.e., 14 days x 24 hours x 15-minute timestep = 1344).

2.4 Lagrangian alongshore connectivity

To understand the pattern of – and difference in - alongshore connectivity from simulations with different mesh resolution, we divided the 306 release sites into 30 nearshore zones extending from the shore to 5 km offshore (Figure 1b). As much as was possible, each zone encompassed nine release sites, but this was not always possible due to the undulating coastline, thus the strength of connectivity between any two zones was weighted by the number of release sites within the source zone. The connectivity between the 30 zones was estimated by recording all particle locations at each timestep throughout the designated 14-day period. As for earlier results, this method incorporates spring-neap tidal variations and releases over waxing and waning stages of the tidal cycle (i.e., includes all 56 particle releases). Two zones were considered connected (i.e., source to sink connection) when a particle released from within a source zone entered a different zone (sink), and self-recruitment was recorded when a particle released from within a zone was recorded within that same zone (at any time during the 14 days from release, i.e., along any particle's entire

trajectory). Although somewhat arbitrary, this approach was consistent for each grid resolution and was considered appropriate since the focus was on comparative general patterns of nearshore connectivity between the runs of different resolutions. To generate the connectivity matrices, the total number of counts within each zone was divided by the number of timesteps within the 14 days. Since the focus is on the comparison of the relative strength and extent of connectivity for the various hydrodynamic model resolutions, for visualisation of the connectivity matrices, this value was normalised by the maximum within the matrix being plotted.

3 Results

3.1 Dispersal and offshore transport

At the mesoscale, the predicted distribution of particles after 14 days was broadly similar between all model resolutions (Figure 4). Particles that were released from exposed and energetic headlands (e.g., the north coast of Anglesey and the Llŷn Peninsula), where tidal flows are strong (e.g., 2-3 m s^{-1}), were advected further offshore and were dispersed more widely after 14 days than those released in quiescent bays where tidal currents are generally weaker (**Figure 3**). This led to fewer particles accumulating around exposed headlands (e.g., around the north of Anglesey), when compared with bays (e.g., Caernarfon Bay) (Figure 4). However, a more detailed comparison revealed clear differences in the simulated transport among model resolutions. For example, in R50, particles released from the northeast coast of Anglesey congregated more densely ~10km directly offshore (red circle in Figure 4), in comparison to the same particles being transported a similar distance in R500, but further to the northeast (blue circle in Figure 4, also illustrated in Figure 6ii). Particles tended to be advected further offshore in R50 than in the coarser resolution models, most notably on the south coast of the Llŷn Peninsula, northwest of Anglesey (e.g., average offshore dispersal distances of 27 km (R50) and 16 km (R500)) and west of the Great Orme.

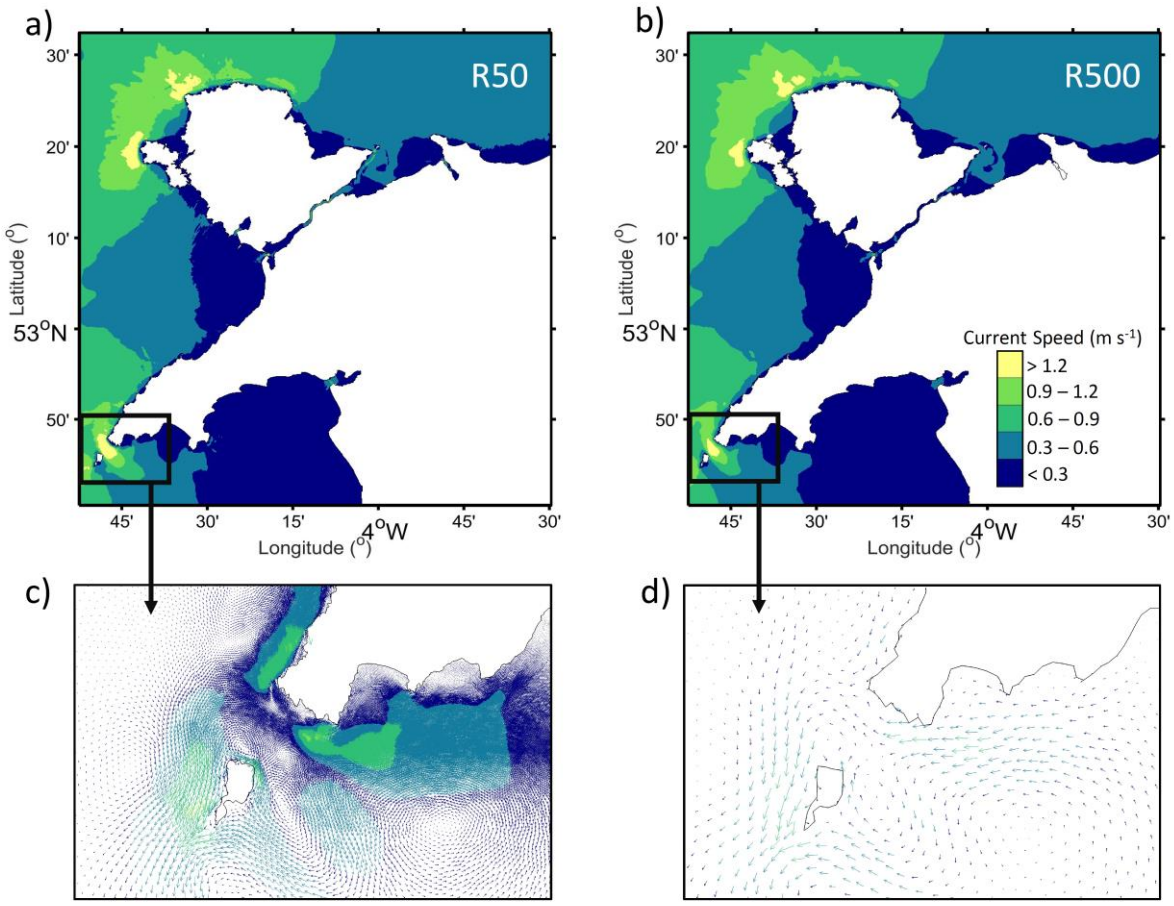

Figure 3. Upper panels: Mean tidal current speeds over a spring-neap cycle for a) high resolution (R50) and b) low resolution (R500) simulations. Lower panels: example residual flow vectors for c) R50 and d) R500 for two days over peak spring tide, where the arrow length and colour indicate the speed, with the colour scale set to match the upper panels.

Offshore transport is considered here as occurring when a particle is transported outside of the 1 km nearshore zone, which is often resolved by only one grid cell (or part of a grid cell) in studies using structured-grid hydrodynamic models (Coscia et al., 2020; Drake et al., 2018; Faillettaz et al., 2018; Wood et al., 2021). The majority of the transport of particles offshore occurred within the first few days after release (Figure 5), with ~30% of released particles transported at least 1 km offshore after one day for all grid configurations (i.e., ~70% remained within the nearshore zone). The finest resolution grid (R50) was the most dispersive, with 30% of all released particles remaining in the nearshore 1 km after 14 days. The coarsest resolution grid (R500) was the most retentive in the nearshore zone, with 46% remaining after 14 days. For the other grids, 34% (R100) and 40% (R250) remained in the nearshore zone. Proportionally, in each of the different grid simulations, more particles were advected offshore from headland release sites (and quicker) than from bay release sites.

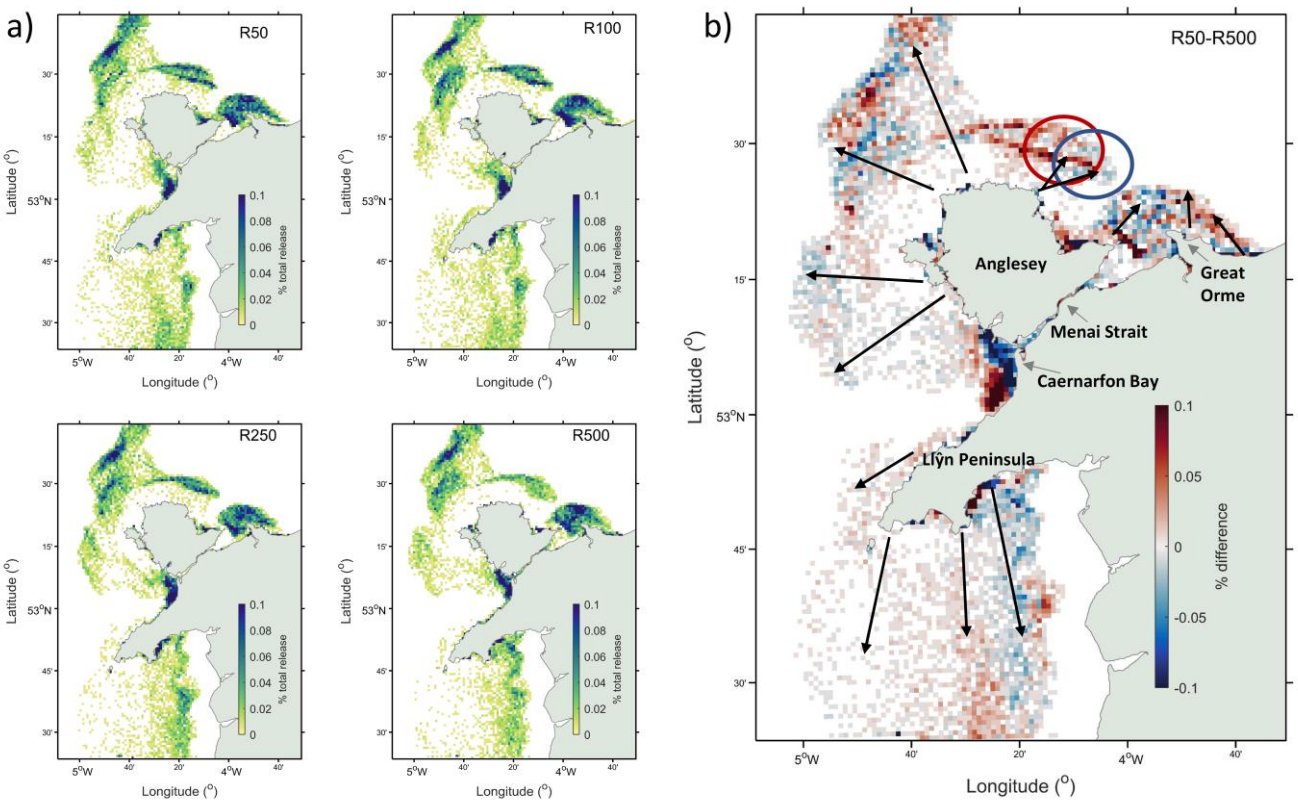

Figure 4. a) Density of particle distribution 14 days from release for R50, R100, R250 and R500, as % of total number of released particles, where yellow indicates low density and green to blue relatively higher density of particle locations. b) Difference in the density of particle distribution at 14 days from release between R50 and R500 (plotted as % density of R50 minus % density of R500, as shown in panel (a)). The red areas represent where more R50 particles were located whereas blue areas represent the locations of more R500 particles. The black arrows illustrate the predominant offshore dispersal direction from various points along the coastline, and the red/blue circles highlight an example of higher densities of particles released from the northeast coast of Anglesey, simulated by R50 and R500, respectively. All densities shown here are on a 1x1 km grid.

The coarser grids tended to produce more particle interactions with the coast, i.e., more particles were simulated as being advected onto land. The percentage of total number of released particles which interacted with the coastline after 14 days were 15% (R50), 14% (R100), 16% (R250) and 18% (R500). Around half of these interactions with the coastline occurred within four days after release from the 500 m offshore release points. When advected onto land, a particle was returned to its position during the previous timestep, resulting in

disproportionately lower total cumulative distance travelled for these particles, which contributed to the relatively lower cumulative distance travelled for the lower resolution grid configurations (Figure 4b). After 14 days from release, the mean cumulative distance travelled by particles released from all sites was highest in R50 and lowest in R500 (Figure 5b), where on average, particles in R50 had travelled >75 km further than those in R500. This pattern is consistent with R50 being the most dispersive grid configuration for particles released within the nearshore zone.

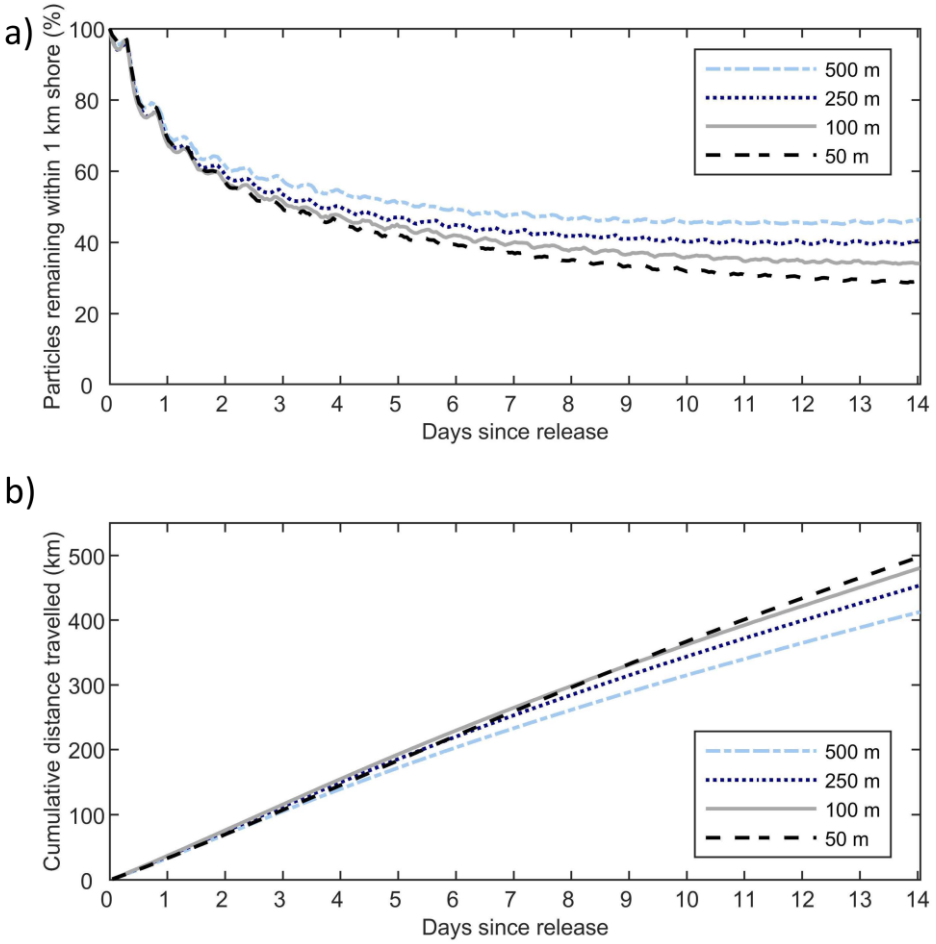

Figure 5. a) Percentage of total number of released particles which remained within the 1 km nearshore zone, for each model grid resolution. b) Average cumulative distance travelled by all particles within each model grid resolution.

3.2 Influence of grid resolution on particle trajectories

The RMSE was calculated for each release location and presented as the mean RMSE per release site over 14 days particle transport (Figure 6). As outlined in Section 2.1, a second

configuration of the high resolution 50 m resolution mesh was generated (using the same resolution constraints as R50, but with triangular mesh elements configured differently), to confirm that the differences in the particle trajectories were due to differences in the model spatial resolution as opposed to an artefact of comparing simulations with different mesh configurations. This comparison confirmed that mesh configuration was not driving the observed differences in the simulated dispersal: e.g., the mean RMSE between these two high resolution R50 grids (after one day) was 40-72% less than for all other grid resolutions compared with R50. Grid resolution had the greatest influence on particle trajectory within the first day from release, with the greatest difference between R50-R500 (mean RMSE of ~2 km) and the difference for R50-R250 and R50-R100 being 82% and 50% of that, respectively. The effect of grid resolution on the difference between particle trajectories (the mean RMSE) tended to decrease with time. As the particles were advected further offshore the RMSEs converged and after one week the mean RMSE values for the three resolution comparisons with R50 were within 5%.

The largest differences in trajectories (relative to R50) tended to occur along sections of exposed coastline and energetic headlands (Figure 6), with the largest differences for particles released from sites 40-70, 140-160, 175-215 (blue ellipses on Figure 6a). Similarly, the lowest RMSE were consistently for particles released within bays. Some example particle trajectories are illustrated in Figure 6i-iv for R50 (black lines) and R500 (blue lines). These are only illustrative snapshots in time, of one particle release from each site (sites (i) 108, (ii) 230, (iii) 250 and (iv) 78), as the differences between the trajectories varied over the tidal cycle. The RMSE was consistently greater for particles released during spring tides, e.g., up to 19% higher for particles released over two days during spring tide in comparison to those released over two days during neap tide (R50 vs R100). Further, with regards to changes in RMSE with time, proportionally the RMSE was greatest closest to time of release (for all resolution grid configurations in comparison with R50). For example, within the first 24 hours from release, a maximum RMSE of 6.8 km (site 155, black arrow on Figure 6a) was calculated for R50-R500. After 14 days, the maximum RMSE (R50-R500) was 25 km (release site 78, blue arrow on Figure 6a), in comparison to a minimum RMSE of 2.3 km at site 6 (in a bay).

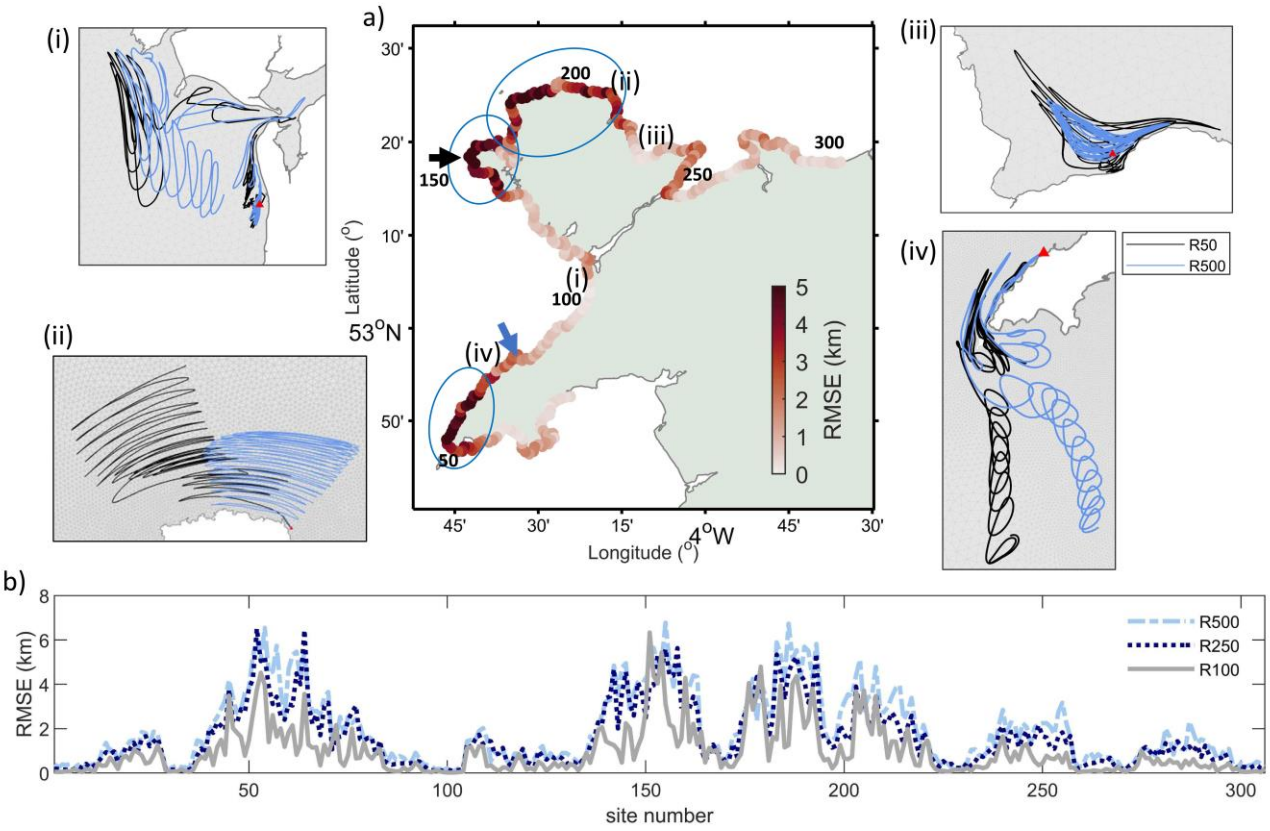

Figure 6. a) Mean RMSE for all releases from each release site for R500 relative to the corresponding trajectories of R50, over 14 days from release, with subplots (i-iv) showing example comparison particle trajectories for R50 (black lines) and R500 (blue lines). Blue ellipses in panel (a) highlight sections of coastline with highest RMSE and the blue/black arrows indicate release sites 78/155, respectively, discussed in Section 3.2. b) Mean RMSE in km for each release site (see Figure 1 for location of numbered sites). Distance in km is the mean absolute difference between the particle coordinates at each timestep throughout 14 days.

3.3 Influences of grid resolution on alongshore connectivity

The schematic of a connectivity network map based on R50 (Figure 7a) illustrates generally a high level of alongshore connectivity of the region. This was expected given the close proximity of the coastal sites (~1 km apart), strong coastal currents (up to 3 m s^{-1}), and the simulated pelagic larval duration of 14 days. The broad pattern of alongshore connectivity (during 14 days from release) was comparable between the four model grids; however, there were differences in the strength of the connections and some key differences in connectivity extent (Figure 7b,c), quantified below.

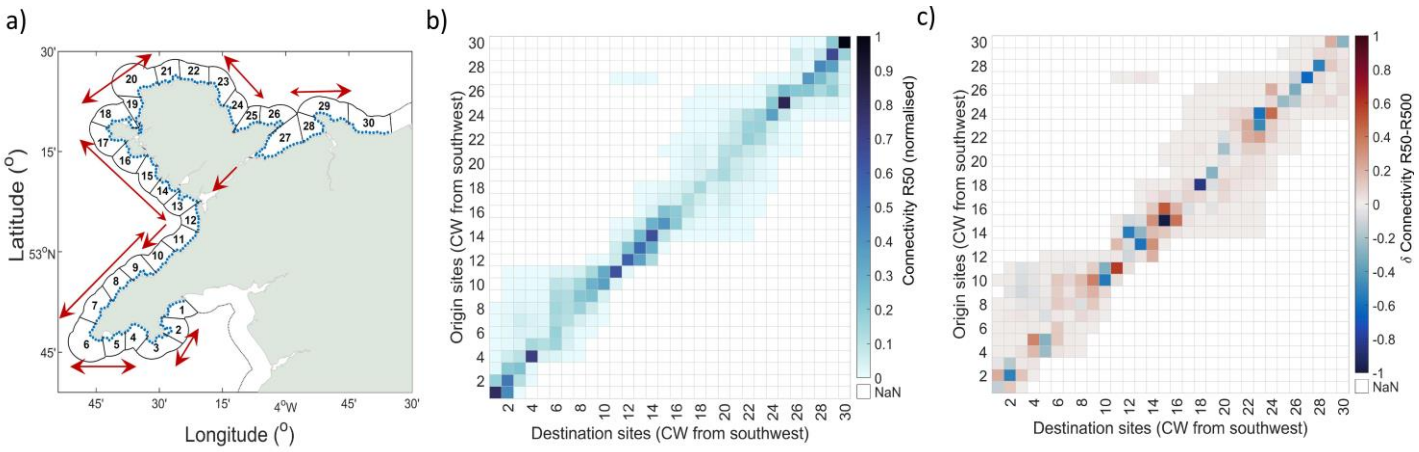

Figure 7. a) Schematic to illustrate dominant alongshore pathways of particles released in the nearshore zone (R50). b) Connectivity matrix for R50, 0-14 days from release. c) Difference in connectivity matrices for high- and low resolution grids, plotted as R50 minus R500 (0-14 days). Both connectivity matrices are calculated as being connections between zones numbered clockwise (CW) from 1-30, and are each normalised by the maximum value in each matrix.

Overall, the total strength of individual connections increased for coarser grid resolutions - R500 had 27% stronger connectivity overall than R50 (R250 was 4% stronger than R50, and R100 had comparable overall strength of connectivity with R50). Notably stronger alongshore connectivity in R500 (blue colours in Figure 7c) occurred in both directions on the southern Llŷn Peninsula (e.g., source-sink zones 3 to 2 and 4 to 5), in the southern mouth of the Menai Strait (source zone 14 to sink zones 12 and 13), and westward along the northeast coast of Anglesey (source zone 24 to sink zone 23). There was also consistently higher alongshore connectivity southwest along the north coast of the Llŷn Peninsula (e.g., source zone 12 to sink zone 11) in R500 in comparison to R50. These zones in which R500 had considerably higher strength of connectivity than R50 tended to be in bays or along relatively quiescent sections of coastline (e.g., zones 2, 5, 10, 11, 25-28). For all grid resolutions, self-recruitment rates were highest in these bays, characterised by shallow water, large intertidal regions and with weak residual flows (<0.05 m s^{-1}). The predominant section of coastline in which R50 had highest alongshore connectivity was along the west coast of Anglesey (zones 14-17), except for at zone 15 where the self-recruitment within R500 was 90% higher, due to an increase in particle interaction with the coastline in the low-resolution model configuration. The maximum strength of connectivity/self-recruitment occurred in zone 30, with R50/R100/R250 predicting around 30% self-recruitment, increasing to 34% for R500. Despite the strongest overall connectivity in the coarsest resolution R500, the total number of connected zones increased

for finer grid resolution, i.e., R50 had 9% more source-sink connections than R500 (although R50 had a comparative number to both R100 and R250, +/<2% difference). There were 37 unique source-sink connections in R50 vs R500 (i.e., where a unique source-sink connection exists in one connectivity matrix but not the other), whereas only 12 unique source-sink connections existed in R500 vs R50. The most significant difference in the connectivity networks was for the R500 simulation (in comparison to the other grid configurations), in the area of the Menai Strait (a tidal channel <500 m wide; see location on Figure 4). In each of R50, R100 and R250, there was residual southwest transport from release zone 27 to sink zones 11-14); however, the R500 simulation was not sufficiently spatially resolved to facilitate transport of particles through the Menai Strait. In R500 the strait was only one grid cell wide, and the simulated tidal currents were unrealistically low, facilitating no transport of particles.

4. Discussion

Many marine species which have pelagic larval stages spawn in the nearshore region, where coastal currents are often complex, with considerable spatio-temporal variation in flow structure. This poses a challenge for biophysical modelling. Here we show that estimates of Lagrangian transport and dispersal in the coastal zone are sensitive to horizontal spatial resolution of the unstructured grid ocean model used. This work highlights the importance of carefully considering the appropriate scales for coastal dispersal simulations. Based on our case study of the North Wales region (UK), biophysical models of relatively coarse spatial resolution (250 m and 500 m) were found to overestimate nearshore retention by up to 50% within the first two weeks from release, compared with finer spatial resolution models (50 m and 100 m). The highest resolution (50 m) simulation was the most dispersive, with particles travelling the greatest cumulative distance (~20% more than the coarsest resolution simulation). Further, the coarser resolution simulations overestimated the strength of connectivity between adjacent coastal regions, while underestimating the potential dispersal range. This work highlights the importance of model setup for dispersal studies within the nearshore zone of topographically complex coastlines.

4.1 Should biophysical models be downscaled as much as possible?

Hydrodynamic model resolution becomes particularly important when considering biologically 'closed systems' that are connected over small spatial/temporal scales (and which are dependent on locally-spawned larvae), in contrast to 'open systems' that are connected over large spatial scales (tens to hundreds of kilometres) and hence can usually be simulated using lower resolution regional-scale hydrodynamic models (Gawarkiewicz et al., 2007). In the nearshore region, hydrodynamic processes differ fundamentally from the deep ocean due to the presence and interaction with the seafloor and the coastline. Coastal and nearshore hydrodynamic processes span a range of spatial scales, including shelf-scale circulation (kilometres – hundredss of kilometres, (Guihou et al., 2018; Holt et al., 2009; Ricker & Stanev, 2020)), river plumes and coastal flooding (several metres – hundreds of kilometres, (Horner-Devine et al., 2015; Kulp and Strauss, 2019; O'Donnell et al., 2008), to small scale surf zone currents and wave processes (several centimetres to tens of kilometres, (Fujimura et al., 2014; Gawarkiewicz et al., 2007; Hally-Rosendahl et al., 2015)). These dynamic processes interact and tend to overlap, presenting a challenge of scale for hydrodynamic modellers. For dispersal studies, the use of long-term and large-domain models with lower resolution (e.g., simulating trajectories over hundreds of kilometres and several weeks/months) is computationally efficient but may not yield the most accurate predictions nor be appropriate in coastal settings. While the spatial resolution of biophysical models has increased in recent years (see Swearer

et al. 2019, and references therein), this increase is not in proportion to computational capacity leading to the question should biophysical models be downscaled further?

For dispersal studies of coastal species, where it is important to resolve high resolution coastal currents, scale matters. Because of practical constraints to modelling (computational, time, data availability etc.), decisions must be made regarding the scales of any modelling study – for example, how many particles should be released, how should the release site be parameterised, over which temporal and spatial scales should the computations be made? Since model resolution (both spatial and temporal) has been shown to affect estimates of direction, distance and relative dispersal of particles (Dauhajre et al., 2019; Hufnagl et al., 2017; Kvile et al., 2018; Lynge et al., 2010; Putman and He, 2013) it is important that we better understand the impact of our chosen spatial scale on estimates of material dispersal (including larval dispersal). Recently, Dauhajre et al. (2019) demonstrated - using a structured grid model – that simulated Lagrangian transport was sensitive to horizonal model resolution. They found that a relatively coarse resolution hydrodynamic model (1 km) failed to resolve the sub-mesoscale shelf currents (predominantly downwelling) of the region (Santa Barbara Channel, California) and concluded that a model of horizonal scale 36-100 m in the nearshore was required. Although the hydrodynamics in the region were considerably different to our shallow and tidally-energetic complex coastline and the hydrodynamic model was a structured grid model rather than the unstructured grid approach that we used, the overarching results agree with ours – i.e., coarse resolution models underestimate offshore transport of material released in the coastal zone.

4.2 Consequences of hydrodynamic model resolution for Lagrangian transport along a topographically complex coastline

The TELEMAC-2D model used here is a two-dimensional depth-averaged tide-only model (see Hervouet, 2007) and so the resolution of the coastal processes are simplified in the vertical plane, e.g., excluding wind- and wave-driven currents and density-driven flows (although the depth-averaged currents take into account reduced flows associated with the bottom boundary layer). Whilst the tide-only model setup reduces the realism of the simulations, it does allow for an initial comparison of the changes in dispersal resulting from decreasing the grid resolution. All efforts were made to minimise any potential artefacts of hydrodynamic model set-up on simulated currents, such as decreasing the model's internal timestep as the model grid resolution became finer, to keep a comparable Courant number (which defines how quickly information propagates through one grid cell). Crucially, the comparison of the two high-resolution (50 m) simulations confirms that it is grid spatial

560 resolution as opposed to grid configuration which drives the differences in simulated particle
561 trajectories, since the RMSE between the two simulations with 50 m nearshore grid resolution
562 was much less than when comparing simulations from coarser resolutions grids (40-72% less,
563 Section 3.2).
564
565 Understanding the processes driving differences in predicted dispersal among models of
566 differing spatial resolution is important in making recommendations on appropriate
567 methodology. Our simulations predicted barotropic tidal currents and their interactions with
568 complex and shallow coastal topography to produce a range of secondary coastal flows such
569 as recirculating eddies and asymmetric fluxes. The velocity fields were resolved in more detail
570 in the finer resolution simulations, owing to the interpolated (smoothed) bathymetry in the
571 coarser models. Intricacies in the residual flow patterns within the first kilometre offshore (and
572 further offshore) were increasingly lost as the grid resolution became coarser. Along the North
573 Wales coastline, there are numerous recirculating features, the simulation/resolution of which
574 was dependent on the model grid spatial resolution (**Figure 3**). Consequently, the highest grid
575 resolution simulations were the most dispersive, contrary to our original hypothesis.
576 Interrogation of the residual flow systems within the nearshore region (not shown) indicated
577 that as a first-order approximation, eddies of the order of the grid scale were resolved, as close
578 inshore as twice the grid scale. For example, circulations on the scale of 50 m were permitted
579 within the first 100 m offshore (R50), increasing to circulations on the scale of 500 m over 1.5
580 km offshore (R500). In R500, several large (>3 km) eddies off the headland of Anglesey were
581 resolved, the centre of each of these was >2 km offshore. However, there were numerous
582 smaller recirculating eddies (<500 m) within the first kilometre offshore resolved in R50 which
583 were entirely unresolved by the R500; these features appear to be driving dispersal offshore
584 rather than resulting in particle retention in the nearshore (i.e., contrary to the original
585 hypothesis).
586
587 Another potential mechanism which explains the important role of model resolution is the way
588 in which coastal complexity is dealt with. Here, the coastline was increasingly less well
589 resolved in the relatively coarser model resolutions and so intricacies of the complex
590 coastlines were lost (where a comparison of the coastline resolution can be seen in **Figure 3**).
591 Where the coastline was less well resolved (R250 and R500 models), there were relatively
592 more (up to 26%) incidences where particles were advected onto land (taken here as water
593 depth <0.1 m) than in the finer resolution simulations (R50 and R100); this effect will have
594 contributed to the coarser resolution simulations being overly retentive in the nearshore zone.
595 Although R50 was the most dispersive simulation, retaining the fewest particles within the 1
596 km nearshore zone, it was R100 which had the fewest particle interactions with the coast,

suggesting that it is not only the detail of the coastline which drives the number of particles being advected onto land but also the resolution of topographic features which will drive some of the fine-scale coastal currents. Particle interactions with land are clearly an important part of predicting dispersal in coastal systems. It is worth noting that the number of coastal interactions was reduced with a decreased particle tracking model timestep (results not shown here), but this had limiting implications for model output because of run time and storage capacity. This highlights the potential sensitivity of simulated dispersal to model timestep, an important consideration for all particle tracking studies. Finally, coarser models by their very nature lead to greater land interactions under simulations where particles are released close to shore. The particles were released 500 m offshore in all simulations, hence in the coarser resolution simulations, they were relatively closer to the coastline (in terms of number of grid cells), which increased the particle-land interactions in the coarser models.

The dispersal patterns from our four different resolution models were broadly similar in each of the simulations, with particles released from the same locations being dispersed in similar directions in each resolution model. However, small differences in larval transport or dispersal distance can have significant implications for the success of marine species to settle and reproduce (e.g., Hold et al., 2021). Our results suggest that predicted dispersal patterns are particularly sensitive to model resolution in tidally energetic regions. We found that the greatest difference in dispersal between the models occurred where particles were released from exposed headlands/islands, e.g., north-western coast of Anglesey, which is highly energetic (tidal currents >3 m/s; Roche et al., 2016). We thus considered whether there was a correlation between the RMSE in the simulated particle trajectories and current speeds or water depth at the release sites but found (results not shown here) no statistically significant correlations. On average, the mean water depth at the release sites was 5% deeper in R50 than in R500 (and 1% and 2% deeper than R100, R250, respectively), an artefact of the interpolation of the high resolution bathymetry onto the lowers resolution grids. That said, in general, the nearshore current speeds were higher in R50/R100 simulations than in the R250/R500 simulations, because of the increased nearshore resolution and higher number of grid cells resolving the current regime more accurately. Further offshore (~5 km), there was minimal current speed difference between the simulations since the horizontal resolution offshore was constrained to be the same a few kilometres offshore. As such, we suggest that using an unstructured grid of <100 m resolution ought to be considered for simulating the transport of material in the nearshore zone.

5. Conclusions

We find that for simulating Lagrangian dispersal of material in the coastal zone of a tidally energetic sea, a spatial resolution of <100 m ought to be used. This study illustrates that estimates of dispersal in the coastal zone were sensitive to ocean models of differing spatial resolutions (50-500 m), implying that careful consideration of appropriate model resolution is important. Relatively coarse resolution models (>100 m) overestimated larval retention in the nearshore zone, underestimated total dispersal distance and therefore led to different estimates of alongshore connectivity (stronger overall connectivity but between fewer discrete source-sink sites) in comparison to high resolution (<100 m) models. This study considered passive particles dispersed over two weeks, and so is relevant particularly to early-life larval stages; however species-specific studies ought to incorporate larval behavioural traits into the particle tracking algorithm, which represents much opportunity for further research. Such studies should also consider natural variabilities in circulation patterns, e.g., from wind-driven and density-driven events. Despite these limitations, our study represents an important contribution to understanding larval dispersal in the coastal zone through simulating potential pathways and connectivity at high spatial resolution. This work is particularly relevant to investigations into the spread of organisms that remain close to shore over timescales of days-to-weeks, e.g., the spread of marine non-native species and pathogenetic parasites, but is equally relevant to simulations tracking the dispersal of eDNA or coastal pollutants such as oil and plastics.

Acknowledgements

This work was supported by the Ecostructure project (part-funded by the European Regional Development Fund (ERDF) through the Ireland-Wales Cooperation Programme 2014-2015). The model simulations were conducted on Supercomputing Wales (a collaboration between Welsh universities and the Welsh Government). Admiralty data were used in the model bathymetry: contains public sector information licensed under the Open Government Licence v3.0. from the UK Hydrographic Office. The ADCP data were collected as part of the SEACAMS and SEACAMS2 projects (part-funded by the European Regional Development Fund through the Welsh Government), available data can be downloaded from: https://portal.imardis.org/. Assistance provided by Guy Walker-Springett was much appreciated.

References

Bode, M., Leis, J. M., Mason, L. B., Williamson, D. H., Harrison, H. B., Choukroun, S., & Jones, G. P. (2019). Successful validation of a larval dispersal model using genetic parentage data. *PLOS Biology*, *17*(7), e3000380. https://doi.org/10.1371/JOURNAL.PBIO.3000380

Horrillo-Caraballo, J.M., Yin, Y., Fairley, I., Karunarathna, H., Masters, I. and Reeve, D.E., 2021. A comprehensive study of the tides around the Welsh coastal waters. *Estuarine, Coastal and Shelf Science*, *254*, p.107326. https://doi.org/10.1016/j.ecss.2021.107326

Coscia, I., Wilmes, S. B., Ironside, J. E., Goward-Brown, A., O'Dea, E., Malham, S. K., et al. (2020). Fine-scale seascape genomics of an exploited marine species, the common cockle Cerastoderma edule , using a multimodelling approach. *Evolutionary Applications*, *13*(8), 1854–1867. https://doi.org/10.1111/eva.12932

Dauhajre, D. P., McWilliams, J. C., & Renault, L. (2019). Nearshore Lagrangian Connectivity: Submesoscale Influence and Resolution Sensitivity. *Journal of Geophysical Research: Oceans*, 5180–5204. https://doi.org/10.1029/2019jc014943

Davies, A. G., & Robins, P. E. (2017). Residual flow, bedforms and sediment transport in a tidal channel modelled with variable bed roughness. *Geomorphology*, *295*, 855–872. https://doi.org/10.1016/j.geomorph.2017.08.029

Davis, A. R., & Butler, A. J. (1989). Direct observations of larval dispersal in the colonial ascidian Podoclavella moluccensis Sluiter: evidence for closed populations. *Journal of Experimental Marine Biology and Ecology*, *127*(2), 189–203. https://doi.org/10.1016/0022-0981(89)90184-6

Demmer, J., Robins, P., Malham, S., Lewis, M., Owen, A., Jones, T., & Neill, S. (2022). The role of wind in controlling the connectivity of blue mussels (Mytilus edulis L.) populations. *Movement Ecology 2022 10:1*, *10*(1), 1–15. https://doi.org/10.1186/S40462-022-00301-0

Drake, P. T., Edwards, C. A., Morgan, S. G., & Satterthwaite, E. V. (2018). Shoreward swimming boosts modeled nearshore larval supply and pelagic connectivity in a coastal upwelling region. *Journal of Marine Systems*, *187*, 96–110. https://doi.org/10.1016/j.jmarsys.2018.07.004

Faillettaz, R., Paris, C. B., & Irisson, J.-O. (2018). Larval Fish Swimming Behavior Alters Dispersal Patterns From Marine Protected Areas in the North-Western Mediterranean Sea. *Frontiers in Marine Science*, *5*(MAR), 97. https://doi.org/10.3389/fmars.2018.00097

Fujimura, A. G., Reniers, A. J. H. M., Paris, C. B., Shanks, A. L., MacMahan, J. H., & Morgan, S. G. (2014). Numerical simulations of larval transport into a rip-channeled surf zone. *Limnology and Oceanography*, *59*(4), 1434–1447. https://doi.org/10.4319/lo.2014.59.4.1434

Gawarkiewicz, G., Monismith, S., & Largier, J. (2007). Observing Larval Transport Processes Affecting Population Connectivity: Progress and Challenges. *Oceanography*, *20*(3), 40–53.

Guihou, K., Polton, J., Harle, J., Wakelin, S., O'Dea, E., & Holt, J. (2018). Kilometric Scale Modeling of the North West European Shelf Seas: Exploring the Spatial and Temporal Variability of Internal Tides. *Journal of Geophysical Research: Oceans*, *123*(1), 688–707. https://doi.org/10.1002/2017JC012960

Hally-Rosendahl, K., Feddersen, F., Clark, D. B., & Guza, R. T. (2015). Surfzone to inner-shelf exchange estimated from dye tracer balances. *Journal of Geophysical Research: Oceans*, *120*(9), 6289–6308. https://doi.org/10.1002/2015JC010844

Hervouet, J.-M. (2000). TELEMAC modelling system: an overview. *Hydrological Processes*, *14*(13), 2209–2210.

Hervouet, J.-M. (2007). *Hydrodynamics of Free Surface Flows: Modelling with the finite element method* (1st ed.). Wiley.

Hold, N., Robins, P., Szostek, C. L., Lambert, G., Lincoln, H., Le Vay, L., et al. (2021). Using biophysical modelling and population genetics for conservation and management of an exploited species, Pecten maximus L. *Fisheries Oceanography*, *30*(6), 740–756. https://doi.org/10.1111/FOG.12556

Holt, J., Wakelin, S., & Huthnance, J. (2009). Down-welling circulation of the northwest European continental shelf: A driving mechanism for the continental shelf carbon pump. *Geophysical Research Letters*, *36*(14). https://doi.org/10.1029/2009GL038997

Horner-Devine, A. R., Hetland, R. D., & Macdonald, D. G. (2015). Mixing and Transport in Coastal River Plumes. *Annu. Rev. Fluid Mech*, *47*, 569–594. https://doi.org/10.1146/annurev-fluid-010313-141408

Hufnagl, M., Payne, M., Lacroix, G., Bolle, L. J., Daewel, U., Dickey-Collas, M., et al. (2017). Variation that can be expected when using particle tracking models in connectivity studies. *Journal of Sea Research*, *127*, 133–149. https://doi.org/10.1016/J.SEARES.2017.04.009

730 Kim, C. K., Park, K., Powers, S. P., Graham, W. M., & Bayha, K. M. (2010). Oyster larval
731 transport in coastal Alabama: Dominance of physical transport over biological behavior
732 in a shallow estuary. *Journal of Geophysical Research: Oceans*, *115*(C10019).
733 https://doi.org/10.1029/2010JC006115

734 Kulp, S. A., & Strauss, B. H. (2019). New elevation data triple estimates of global vulnerability
735 to sea-level rise and coastal flooding. *Nature Communications*, *10*(1), 1–12.
736 https://doi.org/10.1038/s41467-019-12808-z

737 Kvile, K. Ø., Romagnoni, G., Dagestad, K.-F., Langangen, Ø., & Kristiansen, T. (2018).
738 Sensitivity of modelled North Sea cod larvae transport to vertical behaviour, ocean model
739 resolution and interannual variation in ocean dynamics. *ICES Journal of Marine Science*,
740 *75*(7), 2413–2424. https://doi.org/10.1093/icesjms/fsy039

741 Largier, J. L. (1993). Estuarine fronts: How important are they? *Estuaries*, *16*(1), 1–11.
742 https://doi.org/10.2307/1352760

743 Largier, J. L. (2003). Considerations in estimating larval dispersal distances from
744 oceanographic data. *Ecological Applications*, *13*(1 SUPPL.), 71–89.
745 https://doi.org/10.1890/1051-0761(2003)013[0071:cieldd]2.0.co;2

746 Lester, S. E., & Ruttenberg, B. I. (2005). The relationship between pelagic larval duration and
747 range size in tropical reef fishes: a synthetic analysis. *Proceedings of the Royal Society*
748 *B: Biological Sciences*, *272*(1563), 585–591. https://doi.org/10.1098/RSPB.2004.2985

749 Lynge, B. K., Berntsen, J., & Gjevik, B. (2010). Numerical studies of dispersion due to tidal
750 flow through Moskstraumen, northern Norway. *Ocean Dynamics*, *60*(4), 907–920.
751 https://doi.org/10.1007/s10236-010-0309-z

752 Marinone, S. G., Ulloa, M. J., Parés-Sierra, A., Lavín, M. F., & Cudney-Bueno, R. (2007).
753 Connectivity in the northern Gulf of California from particle tracking in a three-dimensional
754 numerical model. *Jounral of Marine Systems*, *71*, 149–158.
755 https://doi.org/10.1016/j.jmarsys.2007.06.005

756 Morgan, S. G., Shanks, A. L., MacMahan, J. H., Reniers, A. J. H. M., & Feddersen, F. (2018).
757 Planktonic Subsidies to Surf-Zone and Intertidal Communities. *Annual Review of Marine*
758 *Science*, *10*(1), 345–369. https://doi.org/10.1146/annurev-marine-010816-060514

759 Nickols, K. J., Gaylord, B., & Largier, J. L. (2012). The coastal boundary layer: Predictable
760 current structure decreases alongshore transport and alters scales of dispersal. *Marine*
761 *Ecology Progress Series*, *464*, 17–35. https://doi.org/10.3354/meps09875

O'Connor, M.I., Bruno, J.F., Gaines, S.D., Halpern, B.S., Lester, S.E., Kinlan, B.P., Weiss, J.M., 2007. Temperature control of larval dispersal and the implications for marine ecology, evolution, and conservation. Proceedings of the National Academu of Sciences (USA) 104,1266–1271. https://doi.org/10.1073/pnas.0603422104

O'Donnell, J., Ackleson, S. G., & Levine, E. R. (2008). On the spatial scales of a river plume. *Journal of Geophysical Research: Oceans*, *113*(C4), 4017. https://doi.org/10.1029/2007JC004440

Pastor, A., Mariani, P., Erichsen, A. C., Hansen, F. T., & Hansen, J. L. S. (2018). Modeling dispersal and spatial connectivity of macro-invertebrates in Danish waters: An agent-based approach. *Regional Studies in Marine Science*, *20*. https://doi.org/10.1016/j.rsma.2018.03.005

Pawlowicz, R., Beardsley, B., & Lentz, S. (2002). Classical tidal harmonic analysis including error estimates in MATLAB using T_TIDE. *Computers & Geosciences*, *28*(8), 929–937.

Pineda, J., Hare, J., & Sponaugle, S. (2007). Larval Transport and Dispersal in the Coastal Ocean and Consequences for Population Connectivity. *Oceanography*, *20*(3), 22–39. https://doi.org/10.5670/oceanog.2007.27

Putman, N. F., & He, R. (2013). Tracking the long-distance dispersal of marine organisms: sensitivity to ocean model resolution. *Journal of the Royal Society Interface*, *10*. https://doi.org/10.1098/rsif.2012.0979

Ricker, M., & Stanev, E. V. (2020). Circulation of the European northwest shelf: a Lagrangian perspective. *Ocean Science*, *16*(3), 637–655. https://doi.org/10.5194/os-16-637-2020

Robins, P. E., Neill, S. P., & Giménez, L. (2012). A numerical study of marine larval dispersal in the presence of an axial convergent front. *Estuarine, Coastal and Shelf Science*, *100*, 172–185. https://doi.org/10.1016/J.ECSS.2012.02.001

Robins, Peter E., Neill, S. P., & Giménez, L. (2012). A numerical study of marine larval dispersal in the presence of an axial convergent front. *Estuarine, Coastal and Shelf Science*, *100*, 172–185. https://doi.org/10.1016/j.ecss.2012.02.001

Robins, Peter E., Neill, S. P., Giménez, L., Stuart, R., Jenkins, S. R., & Malham, S. K. (2013). Physical and biological controls on larval dispersal and connectivity in a highly energetic shelf sea. *Limnology and Oceanography*, *58*(2), 505–524. https://doi.org/10.4319/lo.2013.58.2.0505

Robins, Peter E., Lewis, M. J., Simpson, J. H., & Malham, S. K. (2014). Future variability of solute transport in a macrotidal estuary. *Estuarine, Coastal and Shelf Science*, *151*, 88–99. https://doi.org/10.1016/j.ecss.2014.09.019

Robinson, I. S. (1979). The tidal dynamics of the Irish and Celtic Seas. *Geophysical Journal International*, *56*(1), 159–197. https://doi.org/10.1111/j.1365-246X.1979.tb04774.x

Roche, R. C., Walker-Springett, K., Robins, P. E., Jones, J., Veneruso, G., Whitton, T. A., et al. (2016). Research priorities for assessing potential impacts of emerging marine renewable energy technologies: Insights from developments in Wales (UK). *Renewable Energy*, *99*, 1327–1341. https://doi.org/10.1016/j.renene.2016.08.035

Shanks, A. L. (2009). Pelagic larval duration and dispersal distance revisited. Biological Bulletin 216(3):373-385. *Biological Bulletin*, *216*(3), 373–385. https://doi.org/10.1086/BBLv216n3p373

Simons, R. D., Siegel, D. A., & Brown, K. S. (2013). Model sensitivity and robustness in the estimation of larval transport: A study of particle tracking parameters. *Journal of Marine Systems*, *119–120*, 19–29.

Suanda, S. H., Feddersen, F., Spydell, M. S., & Kumar, N. (2018). The Effect of Barotropic and Baroclinic Tides on Three-Dimensional Coastal Dispersion. *Geophysical Research Letters*, *45*(20), 11,235-11,246. https://doi.org/10.1029/2018GL079884

Swearer, S. E., Treml, E. A., & Shima, J. S. (2019). *A Review of Biophysical Models of Marine Larval Dispersal*. *Oceanography and Marine Biology*. https://doi.org/10.1201/9780429026379-7

Talbot, M. M. B., & Bate, G. C. (1987). Rip current charactersitics and their role in the exchange of water and surf diatoms between the surf zone and nearshore. *Estuarine, Coastal and Shelf Science*, *25*(6), 707–720. https://doi.org/10.1016/0272-7714(87)90017-5

Torrado, H., Mourre, B., Raventos, N., Carreras, C., Tintoré, J., Pascual, M., & Macpherson, E. (2021). Impact of individual early life traits in larval dispersal: A multispecies approach using backtracking models. *Progress in Oceanography*, *192*, 102518. https://doi.org/10.1016/J.POCEAN.2021.102518

Treml, E. A., Ford, J. R., Black, K. P., & Swearer, S. E. (2015). Identifying the key biophysical drivers, connectivity outcomes, and metapopulation consequences of larval dispersal in the sea. *Movement Ecology*, *3*(1), 17.

826 Vasile, R., Hartmann, K., Hobday, A. J., Oliver, E., & Tracey, S. (2018). Evaluation of
827 hydrodynamic ocean models as a first step in larval dispersal modelling. *Continental*
828 *Shelf Research*, *152*, 38–49. https://doi.org/10.1016/J.CSR.2017.11.001

829 Visser, A. (1997). Using random walk models to simulate the vertical distribution of particles
830 in a turbulent water column. *Marine Ecology Progress Series*, *158*, 275–281.
831 https://doi.org/10.3354/meps158275

832 Wood, L. E., Silva, T. A. M., Heal, R., Kennerley, A., Stebbing, P., Fernand, L., & Tidbury, H.
833 J. (2021). Unaided dispersal risk of Magallana gigas into and around the UK: combining
834 particle tracking modelling and environmental suitability scoring. *Biological Invasions*, 1–
835 20. https://doi.org/10.1007/s10530-021-02467-x